Identifying eruptive sources of drifting volcanic ash clouds using back-trajectory modeling of spaceborne thermal infrared data

Daniel B. Williams[1] · Michael S. Ramsey[1] · Daniel J. Wickens[2] · Bobak Karimi[3]

Abstract

A new approach is presented for determining the source region of disconnected volcanic ash clouds using a combination of orbital thermal infrared (TIR) image data, HYSPLIT-generated backward trajectories, and spatial geostatistics. Interpolated surfaces derived from the TIR data are created to find the most likely ash cloud travel path and the potential source volcanoes identified from that path. The ability to use backward trajectories to determine the ash cloud source region will become an important triggering tool to target high spatial resolution orbital sensors, which normally rely on thermal anomalies for new targeting. During cases where thermal anomalies are not present or masked by meteorological cloud, ash cloud detection and predicted source location become more important. Image data from several well-documented past eruptions are presented to validate and determine the overall accuracy of this technique. Because this is seen as a limited range source region validation tool, the ash clouds examined were < 1000 km from their source vent. The approach and analysis are deemed successful if 80% of the model results produce one or more trajectories that pass within 60 km of the source volcano. This methodology could be improved further with the ability to determine the cloud location more accurately using higher image data frequency, and most importantly, greater accuracy in determining the cloud height in the atmosphere.

Keywords GIS · Thermal infrared · Remote sensing · Volcanic ash · HYSPLIT

Introduction

Volcanic systems are complex and controlled by many different processes. Monitoring these systems provides insight into the potential for future eruptions and assessing their hazards. Various precursory signals are used to interpret the movement of magma beneath a volcano and forecast future activity (Sparks et al. 2012). However, many volcanoes worldwide are not permanently monitored from the ground, either due to cost or accessibility, and therefore satellite sensors are routinely employed to provide precursory information for global volcanic activity (Wright et al. 2002). Despite the orbital data availability, volcanoes can produce eruption plumes with little to no precursory thermal warning (Alfano et al. 2011). These plumes can reach heights that impact local to regional populations and can affect commercial aircraft operation (Casadevall 1994). Furthermore, upon injection into the upper atmosphere, these plumes are transported over large areas and in multiple directions, dependent on wind shear and speed (Prata 2009).

The damage caused to aircraft by volcanic ash is well documented (Guffanti and Tupper 2015) and includes abrading of the cockpit windows and exterior, and more dangerously, the full shutdown of engines if silica glass builds up to a point that causes engine flameout (Casadevall 1994). Furthermore, many commercial aircraft flight paths lie directly over active volcanic regions. Those at the greatest risk are in remote areas, such as the North Pacific (NOPAC) region, where more than 100 potentially active volcanoes are present across Alaska, the Aleutian Islands and the Kamchatka Peninsula (Webley 2011). The large volume of air traffic and lack of alternate airports for emergency landings increases this risk (Neal et al. 2009).

✉ Daniel B. Williams
   dbwilliams@pitt.edu

[1] Department of Geology and Environmental Science, University of Pittsburgh, 4107 O'Hara Street, Pittsburgh, PA 15260, USA

[2] ESRI, 1325 Morris Drive, Chesterbrook, PA 19087, USA

[3] Department of Environmental Engineering and Earth Sciences, Wilkes University, 84 West South Street, Wilkes-Barre, PA 18766, USA

Satellite remote sensing provides one of the most temporally and spatially practical tools for the detection and monitoring of volcanic eruptions (e.g., Dean et al. 2004; Ramsey and Dehn 2004; Gudmundsson et al. 2012; Webley et al. 2013) and is becoming the routine method of ash cloud detection (Pergola et al. 2008). No particular sensor exists solely for the purpose of volcanic emissions detection. However, owing to the unique absorption spectrum of volcanic ash and sulfur dioxide (SO_2) in the thermal infrared (TIR; Thomas and Watson 2010), high temporal resolution polar-orbiting satellite sensors such as the Moderate Resolution Imaging Spectroradiometer (MODIS), the Advanced Very High-Resolution Radiometer (AVHRR), and the Atmospheric Infrared Sounder (AIRS) can be used to detect and monitor ash plumes during volcanic eruptions. Although these sensors have relatively high temporal resolutions, they do not provide omnipresent global coverage. Geostationary satellite sensors such as the Imager onboard the Geostationary Operational Environmental Satellite (GOES; Elrod et al. 2003), the Spin Enhanced Visible and Infrared Imager (SEVIRI; Prata and Kerkmann 2007), and the Advanced Himawari Imager (AHI; Bessho et al. 2016) are also used to detect volcanic emissions. They provide data of a specific region of the Earth with even higher temporal resolution (typically 15 min) but at even lower spatial resolutions (> 2 km). Given the quick onset and cessation of some eruptions, coupled with rapid wind speeds, ash-rich plumes can quickly reach several kilometers in the atmosphere (Tupper et al. 2009) and drift well away before any vent activity is detected with orbital data. Therefore, it can be reasonably assumed that short-lived ash-rich columns, such as those produced by vulcanian activity, could quickly disconnect from their source and travel several hundred kilometers before detection, if at all. In addition, more remote volcanoes in the NOPAC region are regularly obscured by meteorological cloud. Algorithms such as MODVOLC and MIROVA, which use the detection of thermal anomalies at volcanoes to track ongoing activity will fail in these instances (Wright et al. 2004; Coppola et al. 2016). Thermal anomaly detection by these automated algorithms as well as data from AVHRR are now also routinely used for the rapid targeting and scheduling of the Advanced Spaceborne Thermal Emission and Reflection radiometer (ASTER; Abrams 2000) through the Urgent Request Protocol (URP) system (Duda et al. 2009; Ramsey 2016). Detection of a thermal anomaly by AVHRR, MODVOLC, or MIROVA triggers an automatic ASTER targeting for that specific volcano. Without this thermal detection, the only evidence of an eruption might be the disconnected, drifting ash cloud. Furthermore, a lack of any collaborating ground or satellite validation may make it difficult to determine the eruptive source region, and hence, an assessment of future activity becomes more difficult.

Our proposed approach for these scenarios is to employ geostatistical modeling of generated backward trajectories. Backward trajectory modeling is commonly applied to volcanic ash plumes to confirm satellite-based derivations of plume height (Winker et al. 2012; Prata et al. 2015). However, this is merely a validation tool to confirm the height of a plume from a known source volcano. In studies of anthropogenic pollution where sources of pollutants are unknown, pollutant concentrations are collected from receptor sites and a concentration-weighted trajectory (CWT) is applied to identify the responsible source (Stohl 1996; Han et al. 2007). To do this, multiple backward trajectories are examined to determine a probabilistic source location. Modeling packages such as Trajstat (Wang et al. 2009) have developed graphical user interface (GUI) tools to aid in this approach. These applications are designed, however, to observe local versus regional sources of pollution in cities, on the timescales of days to years, where the pollutant is measured at a fixed receptor site over a period of time (Cheng et al. 2013; Pietruczuk 2013). Given that an ash cloud-producing volcanic eruption is a temporally short event, and the ash may only be detected by one sensor at any moment in time, these models would be inappropriate and so the method must be modified.

The objective of this study, therefore, is to present a method to track disconnected volcanic clouds back to their source region. We have defined the source region as being within one ASTER scene (60×60 km), as the eventual aim is to use this approach in the ASTER URP program to target the source volcanoes identified. We perform this analysis using a combination of TIR satellite data to first detect the drifting ash and assess its mass, then backward trajectory modeling using the Hybrid Single Particle Lagrangian Integrated Trajectory model (HYSPLIT; Draxler and Hess 1998), coupled with a geostatistical analysis within a Geographic Information Systems (GIS) framework to assess the probable volcanic source region and assess the overall accuracy.

Methods

In the process of searching for applicable ash cloud data, we considered numerous factors including the vast amount of archive data, the source volcanoes, and information on their prior eruptions. Knowledge of the source coupled with any other information on the eruption was considered important for this testing to ascertain the accuracy of the model results. Although many of these eruptions are well characterized in terms of ash mass, cloud height, etc., we want to test our modeling scenario as if the cloud had been first detected by one satellite sensor such as MODIS. From this "initial detection," we initiate the back-trajectory model. Therefore, a series of known eruptions from different volcanoes were used to test the methodological accuracy of the modeling approach

(Fig. 1). We primarily focused on clouds that were < 1000 km from the source vent with the expectation that this tool would be primarily applicable to short-lived eruptions. However, we also selected two ash clouds produced by Puyehue-Cordón Caulle, Chile in 2011 that traveled > 1000 km from their source vent. These test the model's applicability in such an extreme detection scenario.

Data from the MODIS sensor are used to detect the drifting cloud. Whereas MODIS is one of many satellite sensors capable of detecting ash, the data are chosen because of the extensive global coverage and the availability of an appropriate retrieval model (provided by Helen Thomas and Fred Prata, Nicarnica Aviation, Lysaker, Norway; Prata and Prata 2012). There are two identical MODIS sensors on board the NASA Terra and Aqua satellites, each with a spatial resolution of 1 km in the TIR region (Justice et al. 1998). The data have a relatively high temporal resolution and multiple TIR channels, which allow the discrimination of ash from meteorological clouds (Watson et al. 2004). The MODIS data archive (https://ladsweb.nascom.nasa.gov/data/search.html) was accessed to find appropriate data in proximity to the chosen volcanoes following known eruptions. For each eruption, several level 1B radiance data products were acquired. These are processed to detect the presence of ash using methods based upon the brightness temperature difference (BTD) approach, the theory for which is outlined by Prata (1989a, b). The main premise of this method is the differential absorption of ash and water vapor between 11 and 12 μm. The transmission of ash is greater at 12 μm than at 11 μm, whereas water vapor shows the opposite trend. Therefore, by subtracting the 12-μm from the 11-μm channel, negative values result for ash-bearing pixels. There is error associated with this approach depending on the water vapor content of the atmosphere, as well as the potential of ice to coat ash particles (Simpson et al. 2000). These errors can generally be minimized, however, to provide reliable data on ash plume detection (Prata et al. 2001). Additional work over the past 25 years has produced methods for the retrieval of per pixel ash mass loading and ash particle effective radius, using two or three spectral bands (e.g., Wen and Rose 1994; Prata and Grant 2001; Elrod et al. 2003; Pavolonis et al. 2006; Webley et al. 2013). The MODIS ash retrieval model used here was designed for use with SEVIRI data and follows the two-band approach of Prata and Prata (2012). In this model, per pixel effective particle radius, infrared optical depth and mass loading are calculated using the approach of Prata and Grant (2001). However, this model differs slightly to other two-band methods, as surface and cloud temperatures are estimated by using the 12-μm channel brightness temperature. This decreases the number of interpolations required. Once the per-pixel mass loading is calculated, we import it into the GIS framework to provide the input to the geostatistical methods used later in our study.

For data where the plume is still connected to the vent, the distal ash-rich pixels are spatially subset, thus simulating a disconnected cloud for model testing (Fig. 2). Regions towards the furthest distal edge of the cloud are subset further, providing several testing scenarios from one eruption for our approach. A cell grid is placed over each subset section and a point located in the center of each cell. The average ash mass loading of each cell is assigned to that point. These points serve as the coordinates from which the HYSPLIT backward
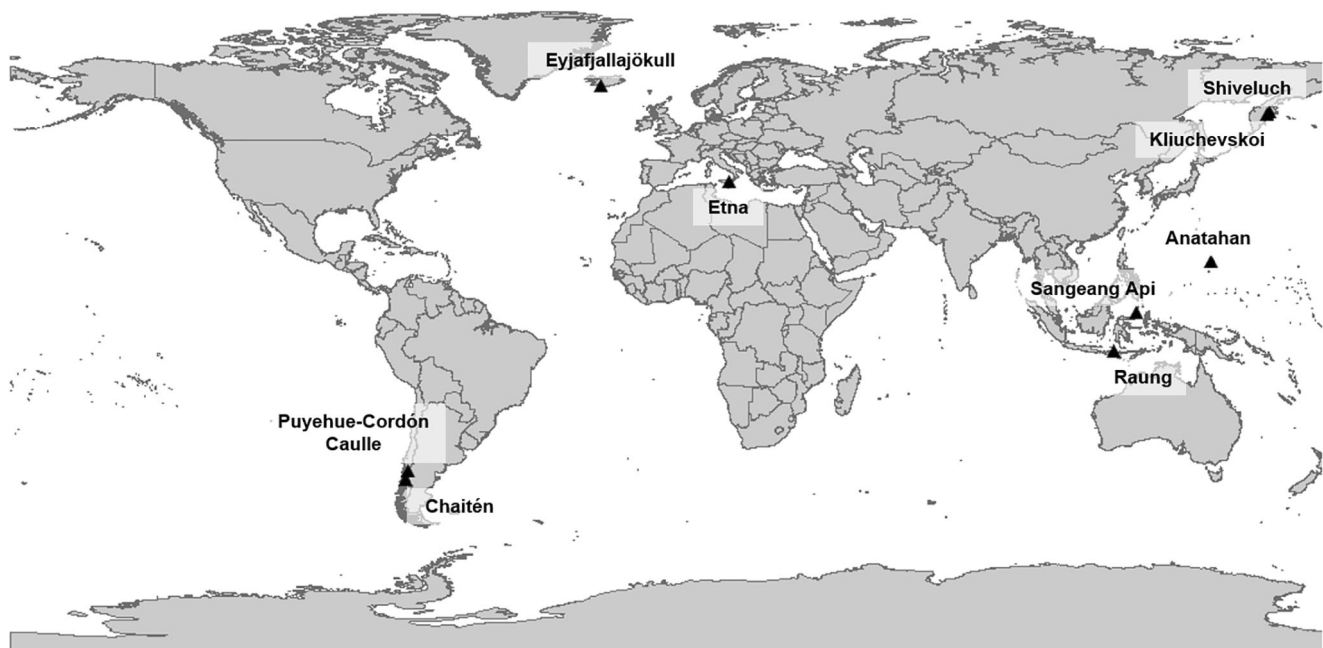

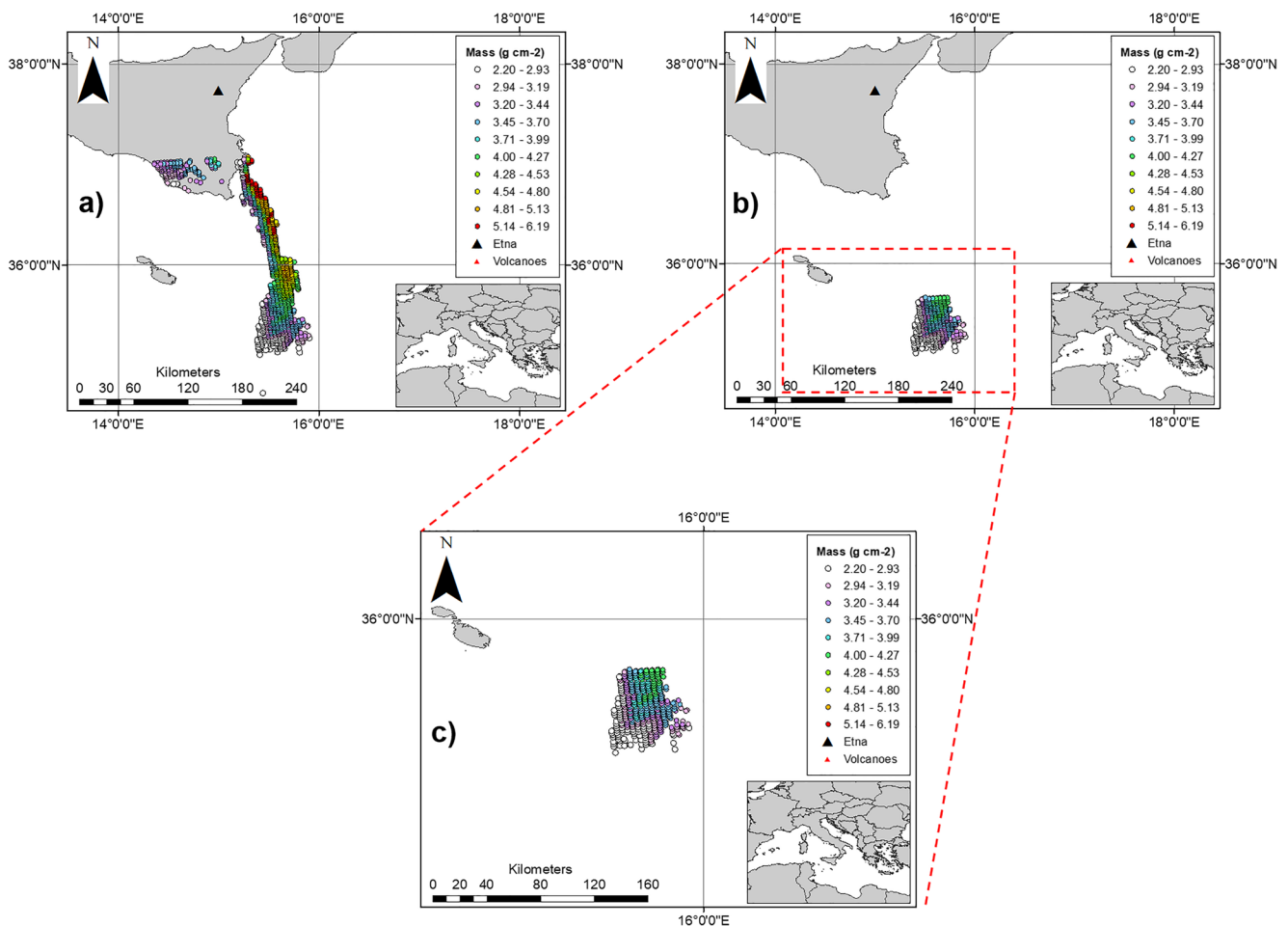**Fig. 1** Location map of the volcanoes used in this study

Fig. 2 Approach for creating a simulated ash cloud disconnected from the source vent using a MODIS retrieval from a Mt. Etna (Italy) ash plume (image date: 28 October 2002 0145 UTC). The ash retrieval model is performed first (**a**) and then a smaller region of this plume is visually identified and separated (**b, c**). From this, the grid is overlain and coordinate points are created and used to initiate the HYSPLIT backward trajectory model

trajectory model is initiated. This sampling aggradation ensured that no bias is imparted in assigning trajectory start coordinates.

HYSPLIT (Draxler and Hess 1998) is a Lagrangian dispersal model that independently calculates the advection and diffusion components of a plume. Lagrangian models are commonly favored where analyzing a single point source for emissions as well as allowing the emission points to be defined at any scale required (Draxler and Hess 1998). The online version of HYSPLIT (https://www.ready.noaa.gov/HYSPLIT.php) is used here, as it is freely available and employs a simple user interface. This version produces data in both shapefile and .kml formats, allowing easy integration into a GIS visualization framework (Fig. 3). The model is setup in "normal" mode, which is one trajectory at each height created from each starting coordinate.

This version of HYSPLIT only allows a maximum of three input starting heights for each trajectory. A more accurate constraint of the volcanic plume height produces fewer possibilities, which in turn should narrow the potential source

regions. This smaller dataset would also be more manageable in a "real-world" scenario, thus improving the targeting accuracy of ASTER. The ash cloud height is first estimated by comparing the 11-μm brightness temperature (BT) of pixels containing ash with radiosonde-measured (available at https://weather.uwyo.edu/upperair/sounding) air temperature (Sawada 2002). This serves as the first assumed height level for the model. However, errors associated with this approach are possible and include: (1) under- or over-cooling of the volcanic cloud upon injection into the atmosphere; (2) higher cloud temperatures recorded as it becomes transparent allowing upwelling radiance from the ground to be detected (Oppenheimer 1998; Webley and Mastin 2009); (3) inaccuracies arising from the distance between the cloud and radiosonde locations (Guffanti et al. 2005); and (4) a difference in time between image and radiosonde data acquisition. Because we are looking at more distal, diffuse plumes, it is assumed that radiosonde data will likely underestimate the plume height, and so a second height level is set above the BT-derived height (termed here BT+), halfway between that

Fig. 3 Trajectories from the ash coordinates shown for three plume altitudes. Obvious trends in direction of travel are seen; however, the BT altitude produced the best fit. The points at each time stamp in the model are used as the input for the EBK geostatistical model
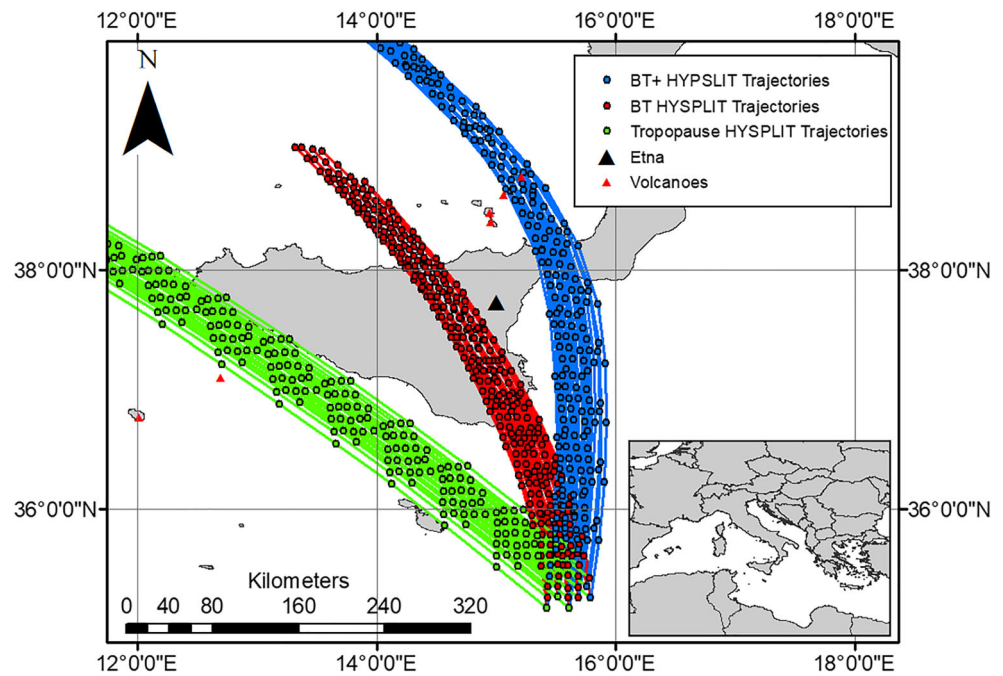
height and the regional tropopause height. The final height used is the local tropopause derived from both radiosonde and AIRS data. AIRS-derived tropopause height data were obtained using the Giovanni online data system, developed and maintained by the NASA GES DISC (Acker and Leptoukh 2007). Both data sources are used to constrain this height level accurately. In many of these scenarios, the radiosonde station was a considerable distance from the ash cloud subset region, whereas AIRS data are obtained near-coincidently with data from the Aqua MODIS sensor. This maximum height is used because previous testing of levels higher than the tropopause demonstrated a significant decorrelation of the plume's travel direction (Williams et al. 2013). Simulations in other studies have also shown that distal ash transport is dominated by atmospheric processes occurring near or at the regional tropopause (Fero et al. 2009). These chosen elevations therefore ensure that the three possible plume heights span the lower, middle, and upper troposphere.

The HYSPLIT-generated trajectories are imported back into the GIS framework, and an Empirical Bayesian Kriging (EBK) approach is applied to interpolate the surface (Fig. 4), used to predict the highest mass loading regions at different times. These regions are considered the most reliable indicator of the overall ash cloud movement. Peripheral regions of the cloud may experience atmospheric turbulence and directional changes, which are beyond the resolution of the HYSPLIT model. The EBK probabilistic method is chosen because of the lower errors associated with its predicted values, which are the result of inclusion of the semivariogram uncertainty, something not done by other Kriging methods (Krivoruchko 2012).

Also, the model constructs the data semivariogram differently. Kriging uses a weighted least squares approach, whereas EBK estimates the semivariogram parameters using restricted maximum likelihood (REML). Trends within the data are located, and once a trend direction for the highest ash mass regions is found, the polygons are isolated to create the final backward trajectory pathway. Lastly, volcanoes within 60 km of this pathway are selected as potential sources.

All data processing and modeling are done using a modest Dell OptiPlex 3060 with an Intel(R) Core(TM) processor at 2.80 GHz. Ash retrieval takes 1–5 min depending on the size of the ash cloud. Ash coordinates are assigned with average mass loadings calculated per grid cell in < 1 min. HYSPLIT data are acquired online, although repeat input of different coordinates and repeat model processing restricts speed. This process is dependent on the number of starting locations chosen, but each set of trajectories can be obtained in < 1 min. Several additional scripts are then run to convert the model output to an ArcGIS useable format. Following this, the EBK model is applied to each of the three height levels and the final trajectories produced. Currently, one set of coordinates can be obtained from an image and fully processed in 15–25 min depending on the number of starting locations. However, with greater automation, a more powerful processor and access to the licensed version of HYSPLIT this time would be greatly reduced.

Results

The model was applied to 40 different scenarios each < 1000 km from the source volcano, with the results categorized

Fig. 4 Surface created by the EBK model. Each trajectory is assigned the mass loading value of its starting coordinate. Points are then generated along this line so the EBK model can be used. This creates an interpolated map of the mass loading. Because higher values are considered more reliable, it is these polygons that form our final trajectories for each height level, provided that a strong trend is visible in the data
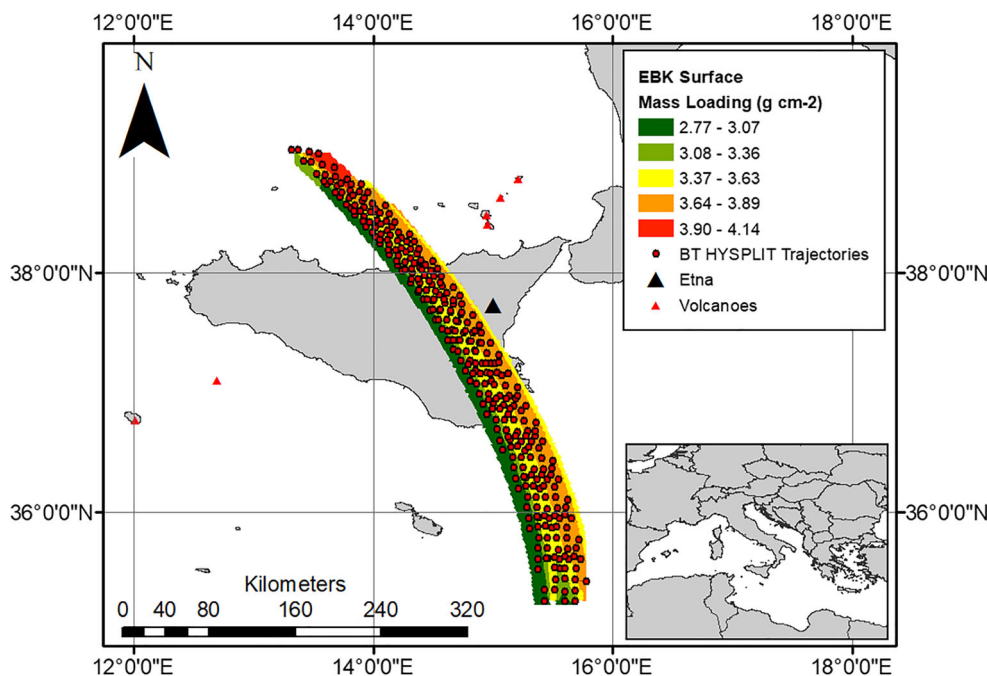
into two different distance ranges (near- and mid-) from the volcano (Tables 1 and 2). The ranges were chosen somewhat arbitrarily but based upon the swath widths of current orbital sensors. For example, the near-range scenarios were defined as those where the cloud is within 185 km of the vent (the Landsat swath width). The mid-range was defined as being between 185 and 2330 km (the MODIS swath width). Results of the extreme back-trajectory test (i.e., > 2330 km distance traveled) from Puyehue-Cordón Caulle are also presented.

Table 1   Results of the modeling approach using the near-range scenario (< 185 km from source)

Minimum distance from cloud to source volcano (km)	Modeled trajectory distance to source volcano (km) using BT height	Modeled trajectory distance to source volcano (km) using BT+ height	Modeled trajectory distance to source volcano (km) using tropopause height
97	73	0	49
98	89	11	99
122	0	3	100
131	150	38	147
131	114	0	138
133	24	12	85
142	14	0	105
163	39	27	154
163	120	6	108
166	0	0	132
168	110	61	81

Near-range model

The near-range model trajectories proved the most accurate, with only one example not tracked back to within the 60-km threshold (Fig. 5). Of these results, the BT+ height was the most accurate, with 10 of 11 backward trajectories tracing the cloud back to within an average distance of 14 km of the known source. The tropopause height was the least accurate for the near-range scenarios, with only one of eight results traced accurately back to within 60 km. The BT-derived height had the greatest range of results, with an average calculated source distance of 67 km. This is directly related to the inconsistencies of the volcanic ash cloud height derived from the BT.

Mid-range model

The mid-range results showed not only a lower level of accuracy, as might be expected (22 of 29 had at least one backward trajectory within 60 km of the known target), but also had the largest number of model scenarios (Fig. 6). The most accurate height was again the BT+, with an average distance of 134 km from the back trajectory to the known source volcano. The overall accuracy of each height decreased significantly compared with the near-range trajectory models, with all heights averaging over 100 km to the source volcano. However, this average is skewed by the most extreme results. In 75.9% of cases, at least one trajectory was traced to within the 60-km threshold. Results from the Kliuchevskoi simulation were particularly interesting, as the tropopause height was the most accurate, producing an average distance from the source

Table 2 Results of the modeling approach using the mid-range scenario (185–2330 km)

Minimum distance from cloud to source volcano (km)	Modeled trajectory distance to source volcano (km) using BT height	Modeled trajectory distance to source volcano (km) using BT+ height	Modeled trajectory distance to source volcano (km) using tropopause height
195	0	6	40
205	64	11	143
214	164	203	61
215	164	192	0
227	137	0	173
237	68	77	234
238	2	49	109
240	204	128	4
247	0	84	54
258	15	49	0
281	32	69	181
296	0	5	197
337	107	29	202
378	10	126	3
381	0	17	81
413	187	65	75
434	88	80	306
480	0	0	0
483	175	39	40
509	84	0	288
510	369	320	13
521	5	11	22
546	0	236	145
557	144	75	338
627	223	10	265
663	25	241	135
669	127	153	179
700	59	0	26
737	382	390	80

volcano of 39 km. This is the only instance where this height produced the most accurate results and shows the possible limitations of relying on height assignments solely from the 11-µm brightness temperature.

Extreme tests

Two extreme tests were performed with mixed results as expected. The first example (Fig. 7) produced excellent results, as each of the trajectories were traced back to within 60 km, despite originating 6752 km from the source. However, a second example at a much greater distance (18,435 km from the source) produced large errors. Both the BT and BT+ height

levels could not be analyzed as the trajectories did not produce a coherent trend, and therefore the EBK model was unable to create a useful interpolated map. The tropopause height level did produce a final trajectory that tracked back to a minimum distance of 1552 km from the source. Despite the improvement using the tropopause height for these very large eruptions, producing accurate trajectories from these large distances is clearly a challenge and not the primary goal of this study.

Discussion

Overall, the model produces reasonable success using the described approach to track volcanic ash clouds back to their probable source vent. However, as with any modeling approach, a detailed discussion of the results is warranted.

Height assignment

Determining the height of a volcanic plume or cloud is critical to understand its propagation from the source, the magnitude of the eruption, and the down-wind hazard impacts to populations on the ground and in the air (Mastin et al. 2009). Plume top height can be determined using an 11-µm TIR band-derived temperature (in this work, MODIS channel 31) assuming the cloud is in thermal equilibrium with the surrounding atmosphere (cf. Holasek and Rose 1991). Therefore, if the atmospheric vertical temperature profile is known, the cloud height can be extracted directly from the temperature data. The atmospheric temperature profile is normally determined using radiosonde data, which is ineffective in certain situations. For example, because the more distal portions of the plume become optically thin, emitted radiance from the ground may also be present in the cloud data. This leads to derived temperatures that underestimate the actual cloud height in the lowest 1000 km of the atmosphere. Although our BT-derived back-trajectory modeling results were relatively accurate (18 clouds tracked to within 60 km of the edifice), this height assignment resulted in a wide distribution of results. This height was, however, expected to perform well for the near-range scenarios, as the plume would presumably be denser closer to the vent, and in theory lead to a more accurate height assessment. The average for this height level for all scenarios was 89 km.

To improve the results, the "BT+" height was used as a proxy for heights midway between the derived BT and tropopause heights. Because the error in BT height will depend on a variety of factors (e.g., ash cloud over/under cooling, amount of ground radiance upwelling, distance of radiosonde measurement to the location of the cloud; Oppenheimer 1998) the assumed BT+ height is defined here as the height roughly midway between the BT-derived height and the regional

Fig. 5 Two examples of the near-range scenarios. **a** An ash cloud from Sangeang Api volcano was captured on 31 May 2014 0235 UTC. The BT and BT+ height levels produced successful backward trajectories. **b** An ash cloud from Shiveluch obtained 6 October 2012 0145 UTC was tracked back to within 60 km by the same two height levels
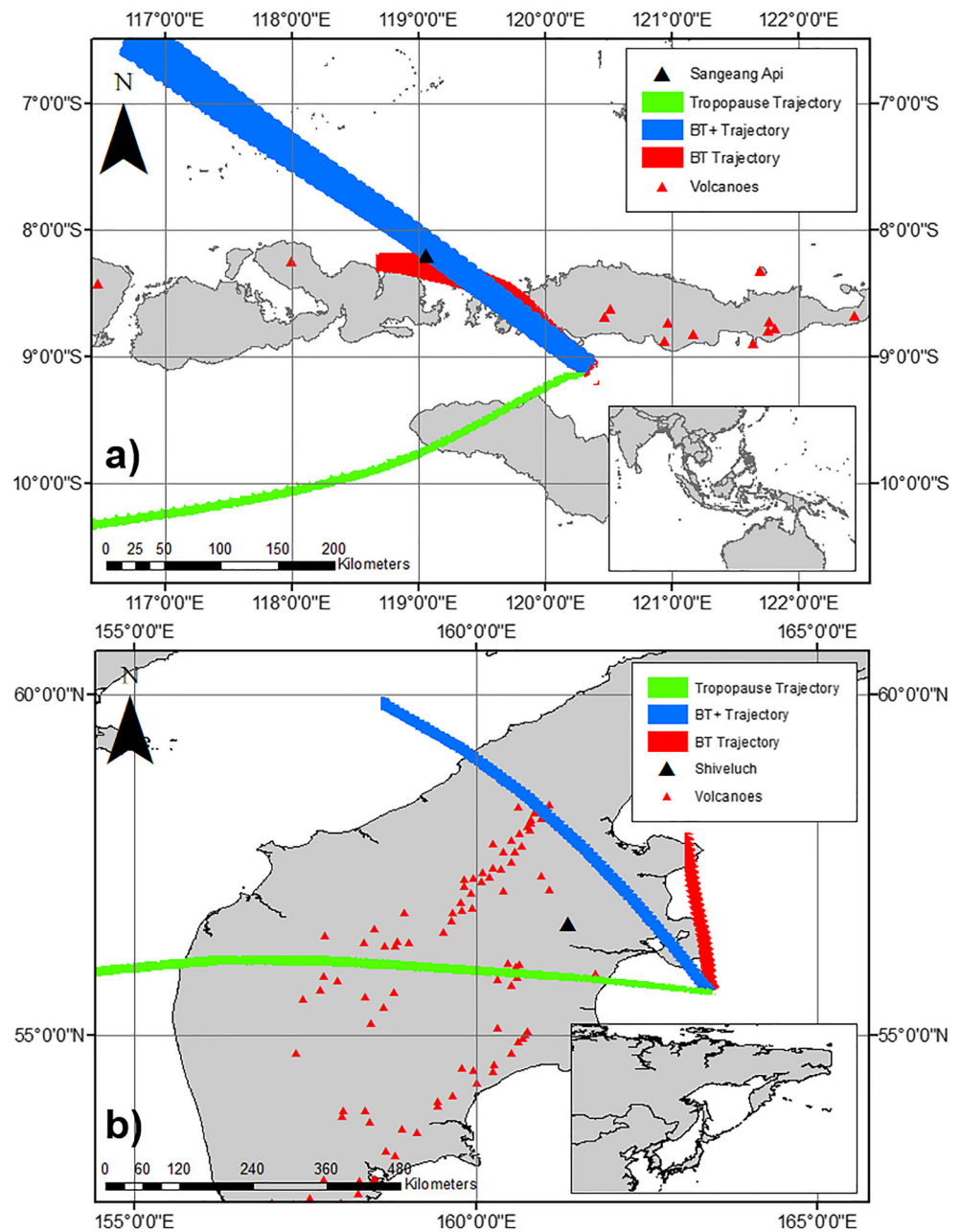
tropopause. In the cases studied here, this height would frequently be ~ 3000 km above the BT-derived height. This height proved to be the most accurate for the back-trajectory model, with an overall average error of 71 km between the model and the actual source. One can therefore assume that most of the clouds examined in this study were drifting at or near this BT+ height.

The tropopause height was the easiest to determine using data from NASA's Giovanni system and radiosonde data. This height resulted in lower model accuracy, with an average distance to the target vent of 115 km. The exceptions to this came from the Kliuchevskoi eruption, where the tropopause height level produced the greatest accuracy (average of 39 km), as

well as the extreme distance cases. In these instances, the eruptions were likely large enough to have reached this layer of the atmosphere.

Having an accurate height assessment would also lower the time needed to analyze a lower volume of data. However, this study has also shown that in some cases, two height levels track the cloud to within 60 km. This does bring into question how accurate the height assessment needs to be, and the resulting potential error. To determine this, trajectories were modeled for an ash cloud produced by Shiveluch, Russia (Fig. 8). The BT-derived height put the plume in the lower troposphere. Backward trajectories were generated every 1000 m between the BT-derived height and the tropopause.

Fig. 6 Two examples of mid-range scenarios. An ash cloud produced by Mt. Etna was captured by MODIS on 28 October 2002 2145 UTC and tracked back to within the 60-km threshold by two height levels (**a**). However, a cloud from Anatahan volcano, captured by MODIS on 5 April 2005 0130 UTC did not produce a successful backward trajectory (**b**)
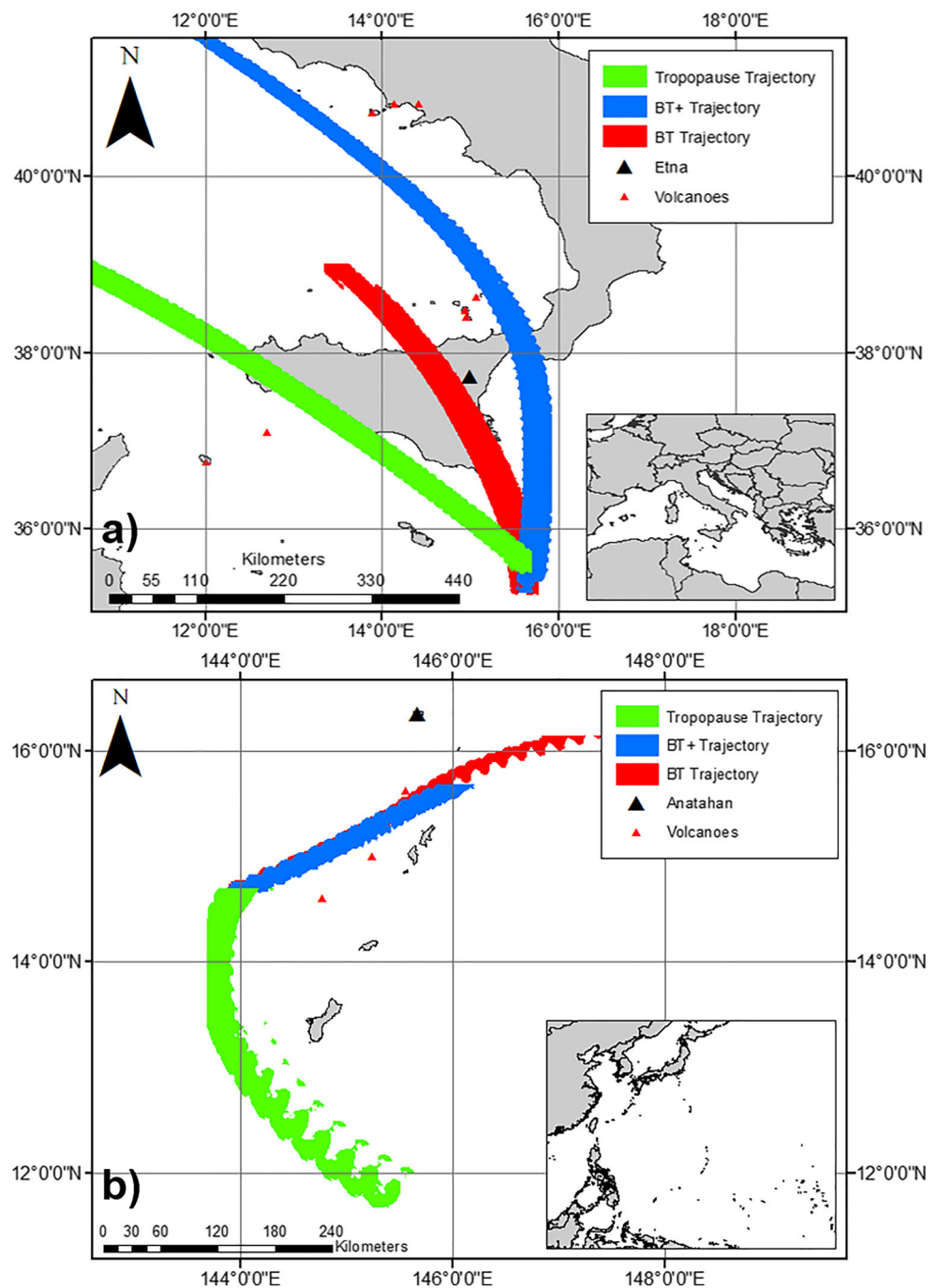
These were then assessed to determine if they met the threshold criteria from the source volcano. The results show that all modeled trajectories between 2397 and 7397 m would still be within the 60-km threshold. This was repeated for an eruption at Anatahan volcano. In this instance, the 60-km threshold was met using a narrower range of heights (2219 to 4219 m). However, this does demonstrate that the model would still be acceptable if the BT height is determined well enough. Other methods of ash discrimination in the TIR may improve the ash cloud height determination. For example, Pavolonis et al.

(2013) outline a three-band method using wavelengths centered at 11, 12, and 13.3 μm on the SEVIRI instrument, to derive ash cloud heights. The height retrievals presented in that study were found to be in good agreement to those obtained by Cloud Aerosol Lidar with Orthogonal Polarization (CALIOP) data. More recent work by Zhu et al. (2017) expands upon this three-band method also using the SEVIRI sensor. Further study is required, however, to compare the height results from these methods to those calculated here and how they would impact the back-trajectory model results.

Fig. 7 Extreme distance example from the Puyehue-Cordón Caulle eruption. The MODIS image was obtained on 8 June 2011 0920 UTC, with the ash plume drifting east below the coast of South Africa
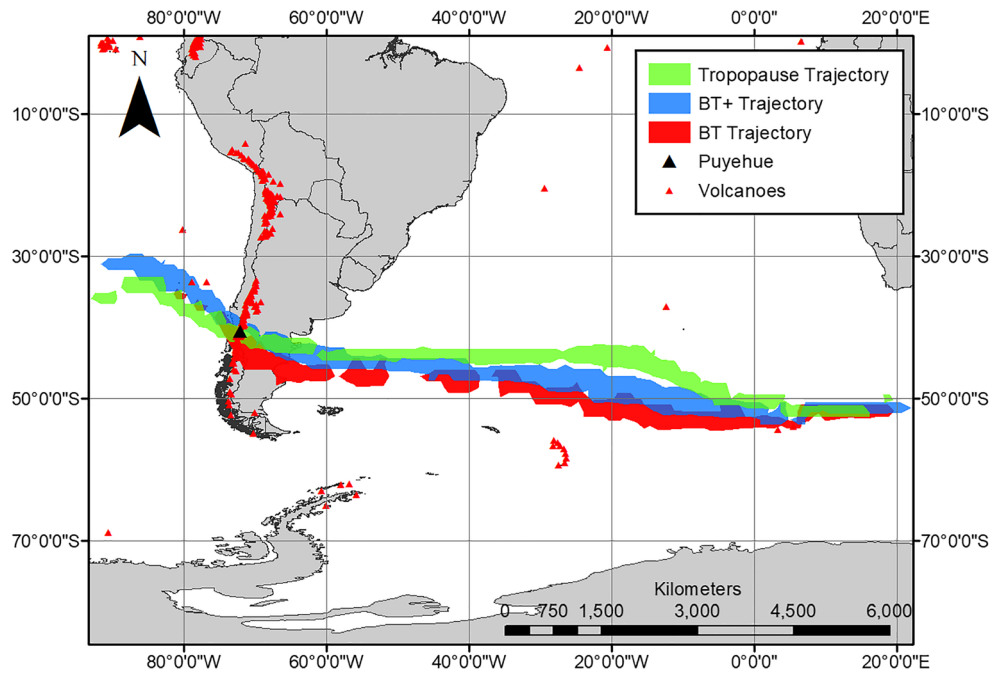
Overall, a correct height assignment is important to successfully locate the source volcano, which would then affect the ability to trigger other orbital data acquisition, such as higher spatial resolution ASTER TIR data (Ramsey 2016). The two-band temperature method has provided generally good results, assuming that a middle troposphere height is also known.

Model uncertainty and geostatistical methods

The HYSPLIT model has proven to be a useful and relatively quick tool, which is essential for rapid response to hazards, but there are limitations that affect the results. Model resolution is a main limiting factor and is the reason why a source region is identified, rather than attempting to track back to a specific

Fig. 8 Model results for the Shiveluch ash cloud detected on 23 November 2014 0225 UTC, where trajectories are generated every 1000 m between the BT-derived height and the tropopause
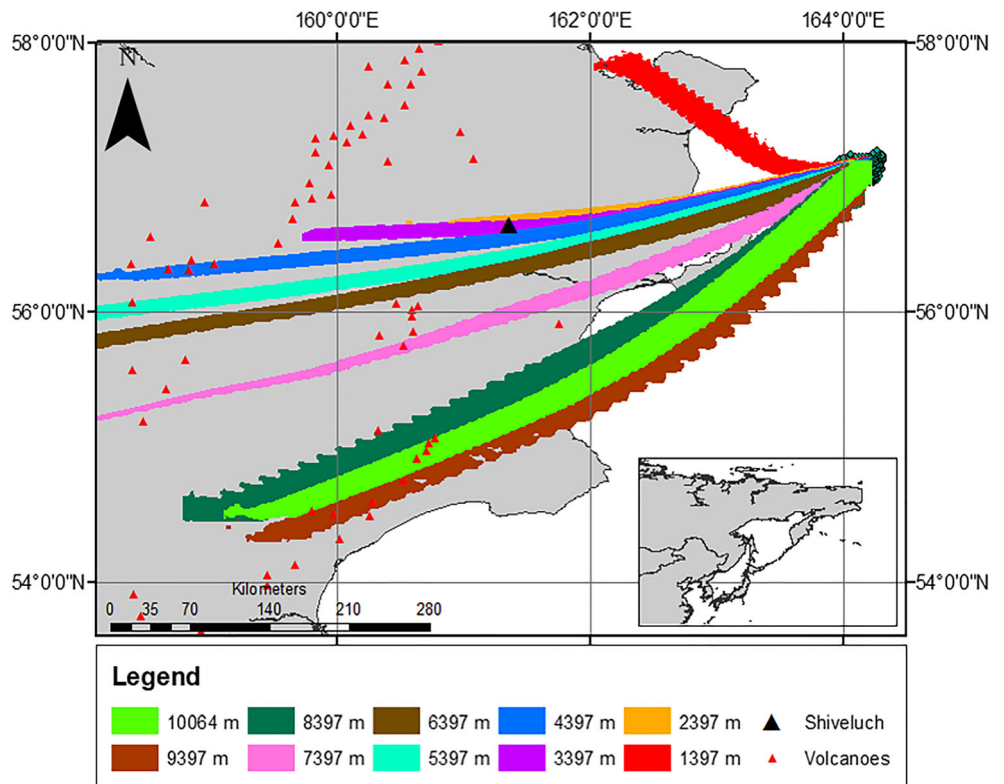
volcanic source. After 2006, the input wind field data for the HYSPLIT model is provided by the Global Data Assimilation System (GDAS). These data have a resolution of 0.5 or 1 degree depending on when the satellite data were collected. Therefore, any atmospheric turbulence or changing wind vectors that occur below this resolution are not resolved by the model. This directly affects the lateral ash cloud distribution and its vertical profile, neither of which are measurable and therefore result in errors to the modeled trajectories. If the ash plume is closer to the edifice, these effects are not as pronounced. For distal and more diffuse plumes, however, the effects of small-scale turbulence will likely have pronounced effects on the modeled ash transport trajectory. This is demonstrated in the results presented here, as an increase in distance between the ash cloud and its source coincides with a decrease in modeled accuracy.

The effects of the back-trajectory model uncertainty will also affect the subsequent geostatistical methods. If an obvious trend is present in the data, a more accurate final trajectory is created and confidence in the predicted location improves. Where model results produce trajectories with no obvious trend, the area covered by the highest mass polygons becomes larger and therefore more potential source volcanoes are included in the final result. This is especially notable for volcanic arcs with closely spaced (and recently active) volcanoes. Because the goal of this approach is to first identify a geographic region and then hopefully further narrow that to a source volcano for further satellite sensor-based analysis, the broad-scale results appear promising but are limited to the data availability and model assumptions. The ability to confidently determine a source region is important, however, as it will aid in subsequent targeting by high-spatial resolution sensors to image new eruptions at improved spatial and/or spectral resolutions, and thus monitor future activity.

Further testing and operational capability

The focus of this work is to use known volcanic eruptions as tests for a series of backward trajectory model results combined with a new geospatial analysis approach to identify an eruption source. The a priori knowledge of each eruption, however, influenced the back-trajectory model run time. In an actual situation where a drifting ash cloud is detected, there may not be knowledge of how long the cloud has been present. Therefore, the next stage in testing of this approach is to prepare a series of blind tests, where the data are subset ahead of time and the model run with no knowledge of the eruption location. This would simulate the best practices for this modeling approach if it were to be used in a future eruption scenario.

The goal here is to postulate how such a model could be integrated into an operational setting. The approach was designed to imitate how an actual fugitive ash cloud would be detected, tracked and assessed. The workflow for the real time version of this model would follow the same routine. First, the cloud would be detected by a higher temporal resolution sensor such as MODIS, with the ash-bearing pixels and the ash mass loading identified and the coordinate grid created. Depending on the ash retrieval model used, ash cloud height would either be derived from the 11 μm BT or using the three-band derived effective height. These heights would seed the HYSPLIT backward trajectory model and the results then imported into the GIS framework. The GIS-generated geostatistical results would be used to identify the potential source volcanoes. The most likely volcanic source would be identified as a target for the scheduling of new data acquisition by the ASTER URP system. These higher spatial and spectral resolution data could then be examined in detail for subtler thermal and compositional changes as well as compared to prior data to assess the potential for future activity (cf. Reath et al. 2016).

Conclusions

A modeling approach combining a two-band BTD determination in TIR satellite data for ash detection, a new geostatistical treatment of the BTD results, and the HYSPLIT model for back-trajectory tracing has been developed and presented. The results are used to statistically predict the backward trajectory of a drifting ash cloud to its most likely source for the purposes of triggering other orbital data acquisitions in cases where no thermal anomaly is detected. This model is tested and shown to be accurate to within 60 km of the known source volcano in 80% of cases, if properly constrained with accurate input parameters such as cloud height, which is the single largest source of possible error.

Being able to constrain the specific geographic region and perhaps even the exact volcanic source of an unidentified eruption is important allowing quick satellite response of other orbital and ground-based assets as well as to direct emergency response to the affected area. Typically, these sensor web approaches using multi sensor observations of a volcanic or fire crisis are triggered by thermal anomalies (e.g., Duda et al. 2009; Coppola et al. 2016; Reath et al. 2016). These detections make for easy targeting of the higher-resolution sensors. However, in cases where an eruption occurs with little to no thermal increase or where that thermal anomaly is obscured, detection of the drifting ash is our next most important indicator of an eruption. Targeting the source of that ash for improved data acquisition from other sensors is the goal. Knowing the source volcano and acquiring those data also provides the ability for further analysis and monitoring over time to infer and predict future activity (Reath et al. 2016). As we continue to develop more accurate methods to both quantify volcanic ash emissions and improve estimates of the

height of volcanic ash clouds, the approach outlined here will increase the number of cases (i.e., > 80%) that yield source locations within 60 km of reality.

References

Abrams M (2010) The Advanced Spaceborne Thermal Emission and Reflection Radiometer (ASTER): Data products for the high spatial resolution imager on NASA's Terra platform. Int J Remote Sens 21(5):847–859

Acker JG, Leptoukh G (2007) Online analysis enhances use of NASA earth science data. EOS Trans Am Geophys Union 88:14–17

Alfano F, Bonadonna C, Volentik ACM, Connor CB, Watt SFL, Pyle DM, Connor LJ (2011) Tephra stratigraphy and eruptive volume of the May, 2008, Chaitén eruption, Chile. Bull Volcanol 73:613–630

Bessho K et al (2016) An introduction to Himawari-8/9—Japan's new-generation geostationary meteorological satellites. J Meteorol Soc Jpn 94(2):151–183

Casadevall TJ (1994) The 1989–1990 eruption of redoubt volcano, Alaska: impacts on aircraft operations. J Volcanol Geotherm Res 62:301–316

Cheng I, Zhang L, Blanchard P, Dalziel J, Tordon R (2013) Concentration-weighted trajectory approach to identifying potential sources of speciated atmospheric mercury at an urban coastal site in Nova Scotia, Canada. Atmos Chem Phys 13:6031–6048

Coppola D, Laiolo M, Cigolini C, Donne DD, Ripepe M (2016) Enhanced volcanic hot-spot detection using MODIS IR data: results from the MIROVA system. Geol Soc Lond Spec Publ 426(1):181–205

Dean KG, Dehn J, Papp KR, Smith S, Izbekov P, Peterson R, Kearney C, Steffke A (2004) Integrated satellite observations of the 2001 eruption of Mt. Cleveland eruption, Alaska. J Volcanol Geotherm Res 135:51–73

Draxler RR, Hess G (1998) An overview of the HYSPLIT_4 modeling system for trajectories. Aust Meteorol Mag 47:295–308

Duda KA, Ramsey MS, Wessels R, Dehn J (2009) Optical satellite volcano monitoring: a multi-sensor rapid response system. In: Ho PP (ed) Geoscience and remote sensing. INTECH Press, Vukovar, pp 473–496

Elrod GP, Connell BH, Hillger DW (2003) Improved detection of airborne volcanic ash using multispectral thermal infrared satellite data. J Geophys Res Atmos 108(D12):4356

Fero J, Carey SN, Merrill JT (2009) Simulating the dispersal of tephra from the 1991 Pinatubo eruption: implications for the formation of widespread ash layers. J Volcanol Geotherm Res 186:120–131

Gudmundsson MT, Thordarson T, Höskuldsson Á, Larsen G, Björnsson H, Prata FJ, Oddsson B, Magnússon E, Högnadóttir T, Petersen GN, Hayward CL, Stevenson JA, Jónsdóttir II (2012) Ash generation and distribution from the April-May 2010 eruption of Eyjafjallajökull, Iceland. Nat Sci Rep 2:572

Guffanti M, Tupper A (2015) Volcanic ash hazards and aviation risk. In: Shroder JF, Papale P (eds) Volcanic hazards, risks and disasters, 1st edn. Elsevier, New York, pp 87–108

Guffanti M, Ewert JW, Gallina GM, Bluth GJS, Swanson GL (2005) Volcanic-ash hazard to aviation during the 2003–2004 eruptive activity of Anatahan volcano, Commonwealth of the Northern Mariana Islands. J Volcanol Geotherm Res 146:241–255

Han Y-J, Holsen TM, Hopke PK (2007) Estimation of source locations of total gaseous mercury measured in New York State using trajectory-based models. Atmos Environ 41:6033–6047

Holasek RE, Rose WI (1991) Anatomy of 1986 Augustine volcano eruptions as recorded by multispectral image processing of digital AVHRR weather satellite data. Bull Volcanol 53(6):420–435

Justice CO, Vermote E, Townshend JRG, Defries R, Roy DP, Hall DK, Salomonson VV, Privette JL, Riggs G, Strahler A, Lucht W, Myneni RB, Knyazikhin Y, Running SW, Nemani RR, Zhengming Wan, Huete AR, van Leeuwen W, Wolfe RE, Giglio L, Muller J, Lewis P, Barnsley MJ (1998) The moderate resolution imaging Spectroradiometer (MODIS): land remote sensing for global change research. IEEE Trans Geosci Remote Sens 36:1228–1249

Krivoruchko K (2012) Empirical bayesian kriging Esri: Redlands, CA, USA. http://www.esri.com/news/arcuser/1012/empirical-byesian-kriging. Accessed 2 August 2016

Mastin LG, Guffanti M, Servranckx R, Webley P, Barsotti S, Dean K, Durant A, Ewert JW, Neri A, Rose WI, Schneider D, Siebert L, Stunder B, Swanson G, Tupper A, Volentik A, Waythomas CF (2009) A multidisciplinary effort to assign realistic source parameters to models of volcanic ash-cloud transport and dispersion during eruptions. J Volcanol Geotherm Res 186(1–2):10–21

Neal C, Girina O, Senyukov S, Rybin A, Osiensky J, Izbekov P, Ferguson G (2009) Russian eruption warning systems for aviation. Nat Hazards 51:245–262

Oppenheimer C (1998) Review article: volcanological applications of meteorological satellites Int. J Remote Sens 19:2829–2864

Pavolonis MJ, Feltz WF, Heidinger AK, Gallina GM (2006) A daytime complement to the reverse absorption technique for improved automate detection of volcanic ash. J Atmos Ocean Technol 23:1422–1444

Pavolonis MJ, Heidinger HK, Sieglaff J (2013) Automated retrievals of volcanic ash and dust cloud properties from upwelling infrared measurements. J Geophys Res Atmos 118:1436–1458

Pergola N et al (2008) Advanced satellite technique for volcanic activity monitoring and early warning. Ann Geophys 51(1):287–301

Pietruczuk A (2013) Short term variability of aerosol optical thickness at Belsk for the period 2002–2010. Atmos Environ 79:744–750

Prata AJ (1989a) Infrared radiative transfer calculations for volcanic ash clouds. Geophys Res Lett 16:1293–1296

Prata AJ (1989b) Observations of volcanic ash clouds in the 10-12 μm window using AVHRR/2 data. Int J Remote Sens 10:751–761

Prata AJ (2009) Satellite detection of hazardous volcanic clouds and the risk to global air traffic Nat. Hazards 51:303–324

Prata AJ, Grant I (2001) Retrieval of microphysical and morphological properties of volcanic ash plumes from satellite data: application to Mt Ruapehu, New Zealand. Q J R Meteorol Soc 127:2153–2179

Prata AJ, Kerkmann J (2007) Simultaneous retrieval of volcanic ash and SO2 using MSG-SEVIRI measurements. Geophys Res Lett 34: L05813

Prata AJ, Prata AT (2012) Eyjafjallajökull volcanic ash concentrations determined using spin enhanced visible and infrared imager measurements. J Geophys Res Atmos 117:D00U23

Prata AJ et al (2001) Comments on "Failures in detecting volcanic ash from a satellite-based technique". Remote Sens Environ 78:341–346

Prata AT, Siems ST, Manton MJ (2015) Quantification of volcanic cloud top heights and thicknesses using A-train observations for the 2008 Chaitén eruption. J Geophys Res Atmos 120:2928–2950

Ramsey MS (2016) Synergistic use of satellite thermal detection and science: a decadal perspective using ASTER. Geol Soc Lond Spec Publ 426:115–136

Ramsey MS, Dehn J (2004) Spaceborne observations of the 2000 Bezymianny, Kamchatka eruption: the integration of high-resolution ASTER data into near real-time monitoring using AVHRR. J Volcanol Geotherm Res 135:127–146

Reath KA, Ramsey MS, Dehn J, Webley PW (2016) Predicting eruptions from precursory activity using remote sensing data hybridization. J Volcanol Geotherm Res 321:18–30

Sawada Y (2002) Analysis of eruption cloud with geostationary meteorological satellite imagery (Himawari). J Geogr Tokyo 111:374–394

Simpson JJ, Hufford G, Pieri D, Berg J (2000) Failures in detecting volcanic ash from a satellite-based technique. Remote Sens Environ 72:191–217

Sparks R, Biggs J, Neuberg J (2012) Monitoring volcanoes. Science 335: 1310–1311

Stohl A (1996) Trajectory statistics-a new method to establish source-receptor relationships of air pollutants and its application to the transport of particulate sulfate in Europe. Atmos Environ 30:579–587

Thomas HE, Watson IM (2010) Observations of volcanic emissions from space: current and future perspectives. Nat Hazards 54:323–354

Tupper A, Textor C, Herzog M, Graf HF, Richards MS (2009) Tall clouds from small eruptions: the sensitivity of eruption height and fine ash content to tropospheric instability. Nat Hazards 51:375–401

Wang Y, Zhang X, Draxler RR (2009) TrajStat: GIS-based software that uses various trajectory statistical analysis methods to identify potential sources from long-term air pollution measurement data. Environ Model Softw 24:938–939

Watson IM, Realmuto VJ, Rose WI, Prata AJ, Bluth GJS, Gu Y, Bader CE, Yu T (2004) Thermal infrared remote sensing of volcanic emissions using the moderate resolution imaging spectroradiometer. J Volcanol Geotherm Res 135:75–89

Webley PW (2011) Virtual globe visualization of ash–aviation encounters, with the special case of the 1989 redoubt–KLM incident. Comput Geosci 37:25–37

Webley P, Mastin L (2009) Improved prediction and tracking of volcanic ash clouds. J Volcanol Geotherm Res 186:1–9

Webley PW, Lopez TM, Ekstrand AL, Dean KG, Rinkleff P, Dehn J, Cahill CF, Wessels RL, Bailey JE, Izbekov P, Worden A (2013) Remote observations of eruptive clouds and surface thermal activity during the 2009 eruption of redoubt volcano. J Volcanol Geotherm Res 259:185–200

Wen S, Rose WI (1994) Retrieval of sizes and total masses of particles in volcanic clouds using AVHRR bands 4 and 5. J Geophys Res 99(D3):5421

Williams D, Ramsey M, Karimi B, (2013) Identifying the volcanic source of disconnected ash clouds using the HYSPLIT dispersion model. In: AGU Fall Meet. Abstr., .p 1538

Winker DM, Liu Z, Omar A, Tackett J, Fairlie D (2012) CALIOP observations of the transport of ash from the Eyjafjallajökull volcano in April 2010. J Geophys Res Atmos 117(D20)

Wright R, Flynn L, Garbeil H, Harris A, Pilger E (2002) Automated volcanic eruption detection using MODIS. Remote Sens Environ 82:135–155

Wright R, Flynn LP, Garbeil H, Harris AJL, Pilger E (2004) MODVOLC: near-real-time thermal monitoring of global volcanism. J Volcanol Geotherm Res 135:29–49

Zhu L, Li J, Zhao Y, Gong H, Li W (2017) Retrieval of volcanic ash height from satellite-based infrared measurements. J Geophys Res Atmos 122:5364–5379